



# Assessment of the LES-WALE and Zonal-DES Turbulence Models in Simulation of the Flow Structures around the Finite Circular Cylinder

R. Kamali Moghadam<sup>1†</sup>, K. Javadi<sup>2</sup> and F. Kiani<sup>1</sup>

<sup>1</sup> Aerospace Research Institute, Tehran, Iran

<sup>2</sup> Sharif University of Technology, Tehran, Iran

†Corresponding Author Email: [rkamali@ari.ac.ir](mailto:rkamali@ari.ac.ir)

(Received December 2, 2014; accepted February 24, 2015)

## ABSTRACT

Three-dimensional unsteady flow field around a finite circular cylinder standing in a flat-plate boundary layer is studied. For this purpose, two different numerical turbulence approaches as wall adapted local eddy-viscosity LES (LES-WALE) and the zonal hybrid RANS-LES approach of Detached-Eddy Simulation (Zonal-DES) are used. Analysis is carried out for a finite circular cylinder with diameter of  $D = 3$  mm and length-to-diameter ratio of  $L/D=6$  which leads to the Reynolds number  $2 \times 10^4$ . Numerical simulation has been performed based on the LES-WALE and Zonal-DES turbulence models using coarse and fine grids. Ability and accuracy of two models in capturing the complex physics of present phenomenon are investigated by comparing their results with each other and validated experimental results. Also, effect of several important parameters such as time-averaged pressure coefficient, velocity, vortex shedding frequency and performance of the LES-WALE and Zonal-DES turbulence models are studied.

**Keywords:** Finite circular cylinder; LES-WALE; Zonal-DES; Turbulence models; 3D unsteady flow.

## 1. INTRODUCTION

The circular cylinder in cross-flow is one of the considerable practical and fundamental fluid-mechanics interests. The flow around finite circular cylinders which one end standing in a flat-plate boundary layer and other end is free have extremely applications in engineering design and make quite complex three-dimensional structure. As shown in figure 1, Agui *et al.* (1992) horseshoe vortex forms at the cylinder-wall junction. These horseshoe vortex can cause material elimination at the cylinder-wall junction, which can lead to the failure of the pier, bridge, and pylon (Pattenden *et al.* 2005; Heseltine 2011). Another major complexity of the flow structure occurs at the free end of the cylinder due to flow interact with the cylinder leading edge at the free end (Afgan *et al.* 2007). Determining of characteristics of the tip vortices near the free end is so important. These vortices created on the lifting surface and dissent from fluid flow causes some undesirable effects (Heseltine, 2011). Furthermore, existence of some other vortices such as arch vortex and trailing vortices (see figure 1) enhances the complexity of these structures and causes a strong turbulent flow around the finite circular cylinder (Pattenden *et al.* 2005; Sumner, 2013). Flow field

structure around the finite cylinder extremely depends on several non-dimensional characteristic parameters. The Reynolds number, height-to-diameter ratio ( $L/D$ ), relative boundary layer thickness of the approach flow ( $\delta/L$ ), and free-stream turbulence are the important parameters in the finite-height case analysis (Krajonvic 2010; Rostamy 2012; Frederich *et al.* 2008). Sumner (2013) performed a strong literature survey on flow structure around the finite cylinders. They also investigated effects of different aspect ratio ( $L/D$ ) and boundary layer thickness ( $\delta/L$ ) on the phenomena which occur on the free end surface or create due to them. They also compared the mean reattachment line position on the centerline of the free end of circular cylinder as function of ( $L/D$ ). Agui *et al.* (1992) analyzed horseshoe vortex, separation, turbulent wake, and transition phenomena. Kawamura *et al.* (1984) showed that how the aspect ratio and the boundary layer thickness affect flow behavior. They also illustrated that the downwash and trailing vortices dominate the vortex shedding pattern. This subject has been also presented in more details by Pattende *et al.* (2005). Giordano *et al.* (2012) experimentally investigated the influence of the Reynolds number and  $L/D$  on heat transfer around the free end finite

circular cylinder using PIV method.

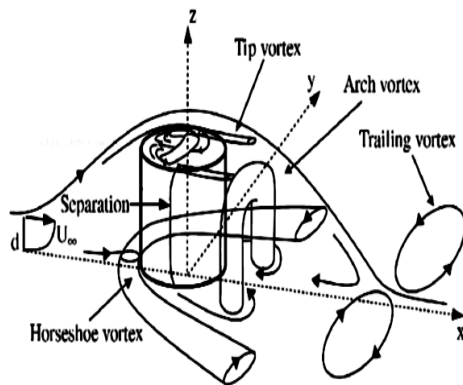


**Fig. 1. Sketch of flow structure around the finite circular cylinder “Agui *et al* (1992)”.**

Recent developments in computational ability of the computers make the CFD tools and the numerical simulations one of the most accurate and reliable methods to investigate complex phenomena. In this case, selecting a turbulence model which accurately predicts the characteristics of the complex flow is so important. Two well-known turbulence models, the LES (Large eddy Simulation) and DES (Detached Eddy Simulation), are extensively used for simulation of the complex flow field. The main objective of the present study is determining ability and accuracy of these two types of turbulence models in capturing complex phenomena over the finite circular cylinder. Since, the two mentioned turbulence models have some problems, especially near the wall, they have been improved several times (Strelets 2001; Spalart *et al.* 1997; Viswanathan 2006; Menter *et al.* 2003). One of the corrected LES method is the wall-adapted local eddy-viscosity LES (LES-WALE) Nicoud *et al.* (1999) and is utilized in the present study. Also, the zonal SST-DES model is one aspect of the improved DES model which quantitatively overcomes to some problems of the standard DES turbulence model Menter *et al.* (2003) and is used in the present paper.

The first large eddy simulation of the finite cylinder flow was done by Fröhlich *et al.* (2004). They simulated flow over the finite cylinder with properties as  $L/D = 2.5$  and  $Re = 4.3 \times 10^4$  and compared their results with experimental data Kappler (2002). Also flow around the free end of the circular cylinder was simulated using the LES-WALE and Zonal-DES at Reynolds number based on diameter of 200000 by Pattenden *et al.* (2007). They compared their results with experimental results which are captured by PIV technique. Frederich *et al.* (2008) used the LES-WALE and Zonal-DES for short cylinder  $L/D = 2$  and showed dependency of their results to  $L/D$ . They also indicated that the LES in an attached laminar boundary layer has better results than the Zonal-DES model. Krajonvic (2010); Pattenden *et al.* (2007) and Afgan (2006) found that flow structure around the circular cylinder is highly dependent on  $L/D$ . Afgan *et al.* (2006) presented the LES of the fluid flows over the finite cylinder and compared

their results by experiment of Park and Lee (2002) where done for  $L/D = 6$  and  $10$  at  $Re = 2.0 \times 10^4$ . One of the recent numerical simulations over the finite cylinder is performed by Krajonvic (2010). He showed marvelous vortex physics near the weak, free end and wall-junction. His simulations at the aspect ratio of  $L/D = 6$  are particularly interesting for the purpose of the present work. Salvador *et al.* (2010) analyzed the LES of their own experimental cases with  $L/D = 2.5$  at  $Re = 4.3 \times 10^4$  and  $L/D = 5$  at  $Re = 2.2 \times 10^4$ . They compared their results for the velocities and turbulence stresses between their experimental observations and the LES simulation. They showed that their simulation for a short wall mounted cylinder predicts the flow has rather agreement with the experimental data. Also, they presented the recirculation zone behind the cylinder and showed that it was slightly over predicted. Baban *et al.* (1991) assessed the unsteady drag and lift forces for the finite short circular cylinder at  $Re = 46000$  and three different circular cylinder with aspect ratios 2, 1.5 and 1. They showed that the unsteady lift force due to oscillating recirculating flow is greater than the unsteady drag force that happens because of the vortex shedding. Liu *et al.* (2005) simulated the flow past the finite circular cylinder with  $L/D = 10$  for a range of the Reynolds numbers from 100 to 200. They used the lattice Boltzmann method and found that for this range, the wake behavior and flow-induced forces are greatly affected by Reynolds number. Also effects of the Strouhal number, mean and root mean square drag, lift coefficients along the span and the Reynolds number on necklace and trailing vortices are studied. Iungo *et al.* (2012) investigated the wake structure generated from a finite height circular cylinder placed vertically on a plane. They found that the mean drag coefficient is roughly invariant by varying the Reynolds number in a range between  $6 \times 10^4$  and  $11 \times 10^4$ . Igbalajobi *et al.* (2012) experimentally investigated the influence of a wake-mounted splitter plate on flow around the surface-mounted of the finite height circular cylinder where the Reynolds number was  $7.4 \times 10^4$ . They studied mean drag force coefficient and the vortex shedding frequency for different  $L/D = 9, 7, 5, \text{ and } 3$  and different lengths of splitter (1 to 7). They found that the splitter plate has insignificant on drag-reduction for finite circular cylinders. Roh *et al.* (2003) studied flow structures at free end surface region of a finite circular cylinder at two different  $L/D = 1.25, 4.25$  and various Reynolds numbers ( $5.92 \times 10^3, 1.48 \times 10^5$ ).

In the present paper, the investigations are carried out over a finite circular cylinder with diameter  $D = 3$  mm and  $L/D = 6$  with the Reynolds number  $2 \times 10^4$ . This complex phenomenon is simulated by both the LES-WALE and Zonal-DES turbulence models using the same coarse and fine grids. Validity and accuracy of the present results are investigated by comparing them with available numerical and experimental data. Comparison between results of the present methods makes important and useful points. According to literature survey, such numerical investigation around the long finite cylinder ( $L/D = 6$ ) by the LES-WALE and

Zonal-DES turbulence models has not been reported.

## 2. PROBLEM DEFINITION AND BOUNDARY CONDITIONS

Three-dimensional unsteady flow field around a finite circular cylinder standing in a flat-plate boundary layer is predicted using two different numerical turbulence approaches; The LES-WALE and Zonal-DES on the same coarse and fine grids. The geometry and flow conditions used in the present study are according to the experiments performed by Park *et al.* (2002). The investigations are carried out using a finite circular cylinder with diameter  $D=3$  mm and  $L/D=6$  which leads to the Reynolds number  $2 \times 10^4$ , approximately. The free stream inlet velocity  $U_0=10$  m/s and the free-stream turbulence intensity in the test section was less than 0.08% by experiment. Because of the strong vortex shedding of the cylinder, downwashes of the free end vortices and complex flow structure, proper computational domain is essential to capture entire flow physics. In the present numerical study the downwash length is placed at  $19D$  and the upstream length is set at  $8D$  far from the cylinder, respectively. The geometry and computational domain applied in the present work are shown in figure 2. The utilized boundary conditions are listed in table 1.

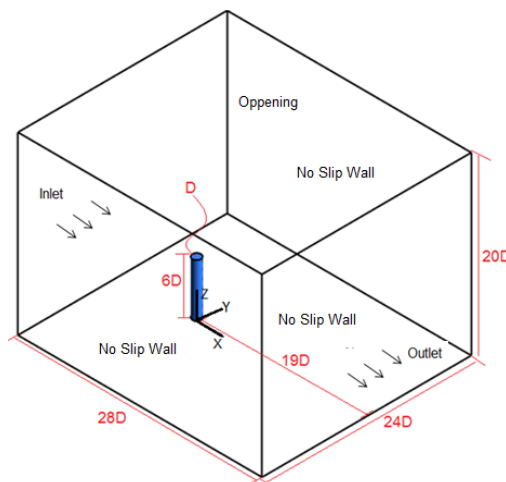


Fig. 2. Geometry and computational domain.

Table 1 Boundary Conditions

Boundary	Boundary Conditions
inlet	uniform velocity profile
outlet	$\partial \bar{u}_i / \partial t + U_\infty (\partial \bar{u}_i / \partial x) = 0$
sides and ceiling	opening boundary condition
wall surface	No-slip boundary condition

## 3. PROBLEM FORMULATION

The 3D unsteady incompressible Navier–Stokes PDE is solved in pressure based form using a cell-centered finite volume on the structured mesh. The central difference discretization, which is second order in time and space, is based on general

curvilinear coordinates. Since the main goal of this study is to determine the accuracy and ability of two known turbulence models to capture the complex flow structures, for summarization, it is avoided to write all of the formulations. Detail of the numerical formulation applied in the present work is available in Strelets (2001); Spalart *et al.* (1997); Menter *et al.* (2003); Lilly (1992); Menter *et al.* (2004); Nicoud *et al.* (1999); Smagorinsky, 1963 and Germano *et al.* (1991).

Several turbulence models are implemented for determining the flow structures around the finite circular cylinder (Williamson 1996, 1985; Zdravkovich 2003; Chen *et al.* 1998). Two applied turbulence models in the present work, the LES-WALE and Zonal-DES, are described in detail in next parts.

### 4.1. Large Eddy Simulation (LES)

The large eddy simulation separates the velocity field into resolved and sub-grid part. The resolved part of the field represents the “large eddies”, while the sub-grid part of the velocity represents the “small scales” whose effect on the resolved field is included through the sub-grid scale model. In this technique, the Navier–Stokes equations are filtered in space, formally defined as the convolution of a function with a filtering kernel  $G$ :

$$\bar{\varphi}(x) = \int_D \varphi(x') G(x, x') dx', \quad \bar{\varphi} = \varphi + \varphi' \quad (1)$$

Where  $D$  is fluid domain, the resolved scale part is  $\bar{\varphi}$  and  $\varphi'$  is the sub-grid scale (SGS) part. Filtering the incompressible Navier–Stokes gives the extra term as sub-grid scale stress,  $\tau_{ij}$ , which is the results of small eddy effects. In this approach, the large scale eddies are directly simulated by the main grid and the discretization scheme. Also, effect of the small eddies are modeled with the SGS. The SGS stress,  $\tau_{ij}$ , is related to the rate of strain tensor,  $\bar{s}_{ij}$ , by the SGS viscosity,  $\nu_{sgs}$ , ( $\tau_{ij} \propto \nu_{sgs} \bar{s}_{ij}$ ). In the LES turbulence model,  $\nu_{sgs}$  simulates just small scale of eddies. Modeling of the SGS viscosity is so important in accuracy and efficiency of a turbulence model. Two known SGS models are explained in the next parts.

#### 4.1.1 Standard SGS Model:

Smagorinsky model “Smagorinsky (1963)” is an algebraic model for the SGS viscosity  $\nu_{sgs}$ . Based on dimensional analysis, the Smagorinsky model for the SGS viscosity can be expressed as,  $\nu_{sgs} = (C_s \Delta)^2 (2\bar{s}_{ij}\bar{s}_{ij})^{1/2}$ , where  $\Delta = (Vol)^{1/3}$  is the grid size and  $C_s$  is the Smagorinsky constant. The coefficient  $C_s$  is not a universal constant and this is the most serious shortcoming of this model. Furthermore, the damping functions close to walls are essential. The shortcoming of the LES+SGS model nSear the wall causes some production of

virtual eddy-viscosity. These problems are modified by several methods in LES. The WALE model is a good technique for this purpose.

#### 4.1.2 WALE SGS Model:

Wall adapted local eddy-viscosity (WALE) used in the present study is also an algebraic model, but overcomes some known deficiencies of the standard SGS model. The WALE model produces almost no eddy-viscosity in wall-bounded flows and therefore is capable to reproduce laminar to turbulent transition. Furthermore, the WALE model has been designed to return the correct wall-asymptotic  $y^{+3}$ -variation of the subgrid-scale viscosity and needs no damping functions. “Nicoud *et al.* (1999)” proposed the SGS viscosity,  $\nu_{sgs}$ , for the unresolved scales by employing the Boussinesq hypothesis, the rate of strain tensor,  $\bar{S}_{ij}$ , for the resolved scales and the wall modeling:

$$\nu_{sgs} = (C_w \Delta)^2 \frac{(S_{ij}^d S_{ij}^d)^{3/2}}{(S_{ij} S_{ij})^{5/2} + (S_{ij}^d S_{ij}^d)^{5/4}} \quad (2)$$

where  $C_w = 0.5$  and the velocity gradient traceless quadratic symmetry tensor,  $S_{ij}^d$ , can be written using the strain rate and the vorticity tensors as:

$$S_{ij}^d = \overline{S_{ik} S_{kj}} + \overline{\Omega_{ik} \Omega_{kj}} - \frac{1}{3} \delta_{ij} (\overline{S_{mn} S_{mn}} - \overline{\Omega_{mn} \Omega_{mn}}) \quad (3)$$

where  $\bar{\Omega}_{ij}$  is the vorticity tensor. This correction makes the LES-WALE model suitable option for the unsteady flows with complex turbulence structure with small-scale processes near the wall where the LES+SGS has some problems. Another method to overcome near wall problems of the LES model is to use the hybrid strategy like the Zonal-DES model.

#### 4.2 Zonal-DES

The difficulties associated with the use of the standard LES models, particularly in near wall regions, have been led to the development of hybrid models by combining the RANS and LES methodologies as a single solution strategy. An example of a hybrid technique is the Detached Eddy Simulation (DES) approach Spalart *et al.* (1997). The time-averaged of the Navier–Stokes equations leads to an additional term called “the Reynolds stress”  $\overline{\rho u_i u_j}$ . By using the Boussinesq hypothesis ( $\overline{\rho u_i u_j} = -2\nu_t \bar{S}_{ij}$ ), this term can be reduced to an unknown proportionally factor  $\nu_t$  obtained here from the  $SST - k - \omega$  turbulence model Menter (1994). Switching between the RANS and the standard LES model is based on a criterion like:

$$\begin{aligned} C_{DES} \Delta > l_{RANS} &\rightarrow RANS \\ C_{DES} \Delta < l_{RANS} &\rightarrow LES \end{aligned} \quad (4)$$

For the structured grid,  $\Delta = \max(\Delta_x, \Delta_y, \Delta_z)$  is suitable and turbulence length scale is  $l_{RANS} = k^{1/2} / \beta_k \omega = k^{3/2} / \varepsilon$ . The constant  $C_{DES} = 0.61$  is obtained by calibration against decaying isotropic turbulence. Based on this definition, the standard DES model is highly dependent to the grid quality. This grid sensitivity causes some problems which can be explained in two categories:

##### 1) Grid Induced Separation (GIS):

The main problem of the standard DES is lack of a mechanism to prevent activation of limiter in the boundary layer. It happens when the SGS is smaller than the boundary layer thickness. This problem causes unphysical and undesirable (grid-induced separation) results (Menter *et al.* 2003; IM *et al.* 2011). It is also showed by Menter *et al.* that the SST-DES limiter affects the RANS model and moves the separation point upstream relative to the original SST model. Spalart *et al.* (2006) named such problems the DES model as “ambiguous grids” and showed that the DES would “fake” some effects that should be properly obtained from RANS.

##### 2) Interface challenges:

Second important elements of hybrid models are interface conditions, which convert turbulence from unresolved mode (RANS) to resolved mode (LES). Appropriate condition at the interface for the variables used in the transport equations of the RANS model needs careful calculation from the available LES data. Not only smoothing of eddy viscosity, but also the modeling constants across the transition zone with the continuity constraint at the interface location is also required. It is desirable to fix the interface in such manner which to be independent of the grid size. In such condition this method is applicable for complex geometry and separated flows. For example, explicit specification of interface location is obviously not a desirable one. The location should be automatically choose based on the local grid information without imposing further limitation on grid in other directions Vengadesan *et al.* (2007). For fine grids, the switch from RANS to LES can take place somewhere inside the boundary layer and produce a premature grid-induced separation Menter *et al.* (2004). In contrary, “Philippe *et al.* (2001)” was mentioned that in using of the DES model, as the grid coarsens, the DES length scale and the eddy viscosity grows, and destruction terms subsides.

These limitations of the standard DES model lead to some modification for DES models. For example, in order to avoid the GIS problems of the standard DES model, the standard DES concept has been extended to Delayed-DES (DDES) Menter *et al.* (2003). Also, Spalart *et al.* (2006) were modified the DES model to overcome some of the shortcomings related to the standard DES grid. Another modification for preventing from the GIS problems in the standard DES model is the Zonal-DES proposed by Strelets (2001). They modified the DES model by reformulating the dissipation

term:

$$\varepsilon = k\beta_k\omega \text{ is replaced by } \varepsilon = k\beta_k\omega.F_{DES} \quad (5)$$

where:

$$F_{DES} = \max\left(\frac{l_t}{(C_{DES}\Delta)}, 1\right) \quad (6)$$

and  $F_{SST} = 0, F_1, F_2$  and  $F_1=0, F_2=1, C_{DES} = 0.61$  and  $\beta_k = 0.075$  described with details in ref. “Strelets (2001)”. All results of the present study are performed using this modification.

### 5. COMPUTATIONAL DOMAIN

Two types of structured coarse and fine grids have been used to predict the flow field around the finite circular cylinder. Total element of coarse grid is 4,880,000 and that of fine grid is 12,740,000. Due to fair comparison, these grids are the same for both simulations of the LES-WALE and Zonal-DES turbulence models.  $Y^+$ s ( $Y^+ = \rho u^* y / \mu$ ) calculated in the simulations are listed in table 2.

**Table 2  $Y^+$  calculated in the simulations**

Turbulence Model	$Y^+$ range
LES-WALE (Coarse grid)	3.35-49.17
Zonal-DES (Coarse grid)	5.43- 69.18
LES-WALE (Fine grid)	0.28-16.44
Zonal-DES (Fine grid)	1.54-29.87

The time step is chosen as 0.00005 which creates minimum courant number (CFL) 0.08 and 0.037 for the coarse and fine grids, respectively. The selected time steps are the same for both the LES-WALE and Zonal-DES models. To achieve stable conditions, simulations have been done for 48000 time steps to pass the inlet flow through the entire computational domain for 5 times. The results are presented for statistical time averaged of the last 8000 time steps.

### 6. RESULTS AND DISCUSSION

#### 6.1 Pressure and Velocity Distribution

Figure 4 shows comparison of the time-averaged surface pressure coefficients at different horizontal sections along the cylinder for both the turbulence models with the experimental data (Park *et al.*, 2002). For the coarse grid, both the turbulence models do not have appropriate agreement with the experimental data and predict the pressure recovery region slower than the experimental results. For the fine grid, the LES-WALE turbulence model has good agreement with the experimental data in all sections, but results of the Zonal-DES model has not significant difference with those of the coarse grid. It is noted that for both the coarse and fine grids, the Zonal-DES turbulence model has more delay in capturing of the recovery region than the LES-WALE model. Visualization of the streamlines on the cylinder shell for both the simulations in figure 5 indicates the flow behavior on back of the cylinder. The mentioned delay is also seen at

prediction of the separation position for the Zonal-DES turbulence model (See table 3).

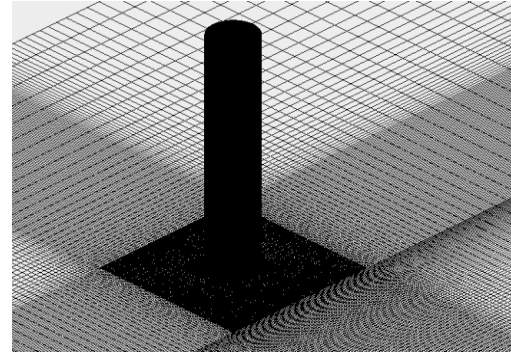


**Fig. 3. Computational grid.**

**Table 3 Comparison of the separation position**

Turbulence Model	separation position
LES-WALE	100°
Zonal-DES	115°

The main reason of the poor results of the Zonal-DES model returns to quality of the applied grid near the wall. By measurement of size of the coarse grid and the RANS turbulence length scale near the wall, it is found that the criterion  $C_{DES}\Delta < l_{RANS}$  is always true for the present case therefore the RANS model is not active near the wall and the Zonal-DES always switches to the LES model (see Eq. 4). Also, results calculated by the fine grid are worse than those by the coarse grid. It should be noted that the LES models used for the Zonal-DES is the original LES without any modifications near the wall. As mentioned before, the shortcoming of the original LES model near the wall causes some added production of eddy-viscosity near the wall while the LES-WALE model overcomes this problem and produces almost no eddy-viscosity in wall-bounded flows. Comparison of the turbulence eddy viscosity iso-surfaces for both models in figure 6 confirms this matter. This incorrectly produced eddy viscosity in the attached boundary layer causes an imaginary turbulent behavior and delayed separation (Strelets, 2001; Frederich *et al.*, 2008).

An interesting point in fig. 4 (particularly for  $Z/L=0.5$ ) is two peaks in recovery regions of the LES-WALE results using the fine grid. These two peaks are in agreement with two Strouhal numbers and two tip vortices of the flow over the finite cylinder (Johnston *et al.*, 1996; Hain *et al.* 2008) where also reported for a short cylinder by Frederich *et al.* (2008). When the first tip vortex is formed in one side of the separation point, its pair begins to form in other side. The first tip vortex has the exceeded energy toward its pair. Therefore, the tip vortex with greater energy causes the main separation point of the cylinder as  $St_1$  and its pair with lower energy creates secondary separation or second peak pressure coefficient as  $St_2$  (see Figs. 7 and 24).

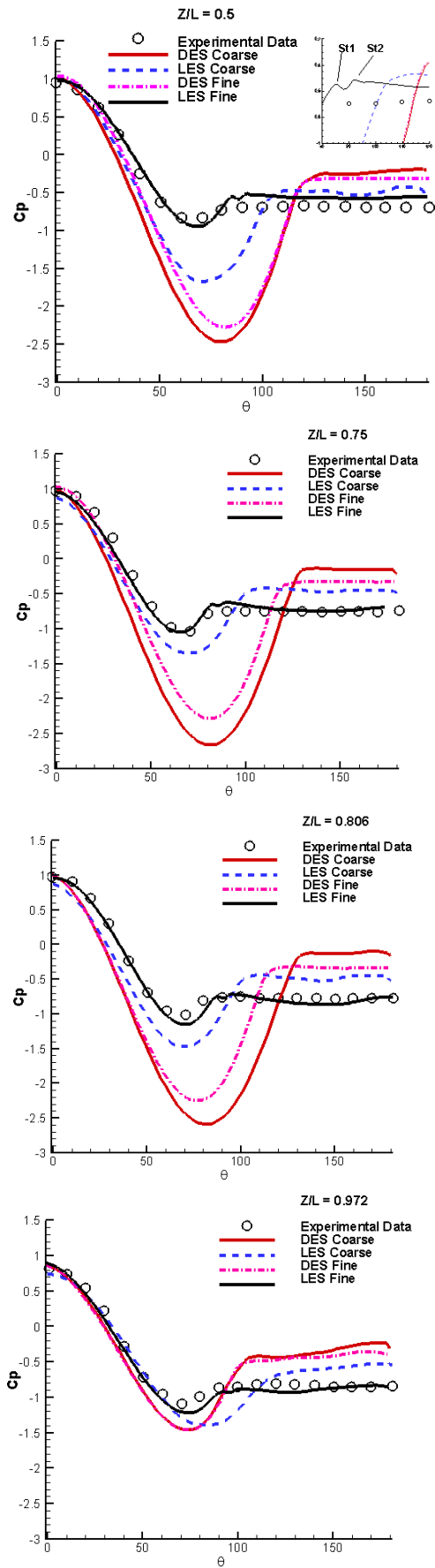


Fig. 4. Surface pressure coefficient at different  $z$  locations.

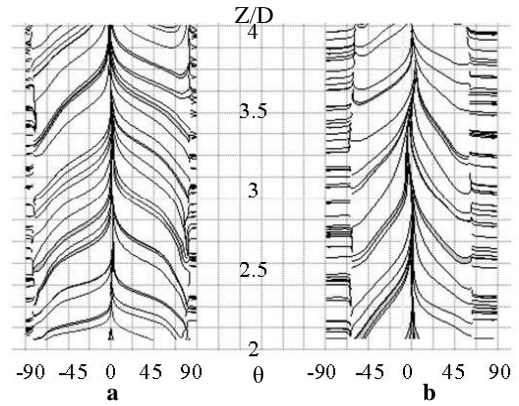


Fig. 5. Visualization of streamlines on the cylinder shell, (a) LES-WALE (b) Zonal-DES ( $X/D=0.5$ ).

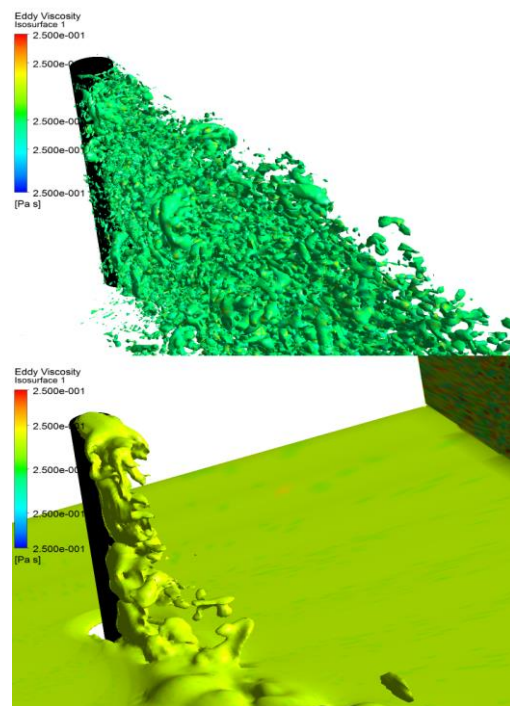


Fig. 6. Comparison of the turbulence eddy viscosity iso-surfaces, (a) LES-WALE, (b) Zonal-DES.

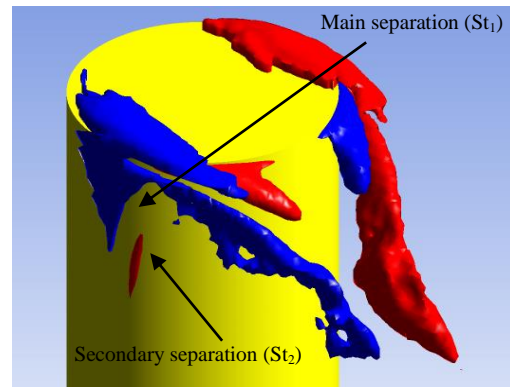
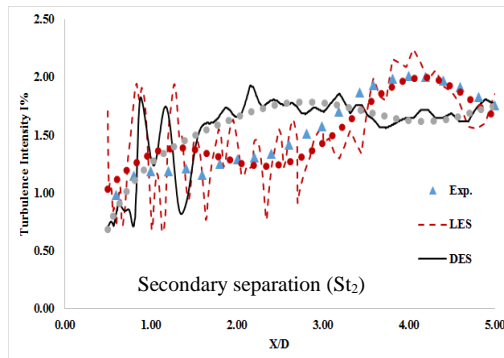


Fig. 7. The main and secondary tip vortex plotted by vorticity  $x = \pm 1500 [s^{-1}]$ .

The turbulence kinetic intensity captured by both

the present turbulence models using the fine grid are compared with available experimental data (Park *et al.*, 2000) in figure 8. For better comparison of the results, the polynomial curves are plotted between data calculated by both the turbulence models. The results show more accuracy of the LES-WALE model respect to the Zonal-DES turbulence model. Figure 9 compares profiles of the streamwise mean velocity and related fluctuations for both the turbulence models using the fine grid with the numerical (Fröhlich *et al.*, 2004) and experimental data (Kappler, 2002) at different sections. The LES-WALE turbulence model has better agreement with the experimental and numerical data than the results of the Zonal-DES turbulence model.



**Fig. 8. Comparison of the vortex formation region at  $Z/L=0.5$ .**

### 6.2 Flow Structure

To show flow structure around the finite cylinder, firstly, near wakes visualized by streamlines in plane  $y=0$  are compared for both the LES-WALE and Zonal-DES models in Fig. 10. The free end vortices are seen in both the simulations. The free end vortex in the LES-WALE model is captured sooner than that of the Zonal-DES model. It creates a smaller vortex in back of the cylinder near the free end. Generally, premature eddy viscosity produced by the Zonal-DES model gives a smaller reattachment region than the LES-WALE model. This phenomenon moves the saddle point of the back flow upper than its location predicted by LES-WALE. Time averaged velocity streamlines of the fine grid are plotted in figure 11 at XY-plane for various  $Z/L$  locations. It is interesting to note that a pair of narrow recirculation bubbles in the wake region generates a strong wide back flow (towards the cylinder). This is significantly different pattern from the infinite cylinder (Afgan, 2007). It is clearly observed in figure 11 that at lower free end of the cylinder, the Zonal-DES model has delay in prediction of separation position and also makes smaller recirculation region than the LES-WALE model. As mentioned before, this is because of the shortcoming of the DES model in producing the imaginary eddy viscosity and making smaller recirculation region. At  $Z/L=1$ , the flow structure at the free end of the finite cylinder is compared for both the LES-WALE and Zonal-DES model simulations. It is shown that saddle line of the

Zonal-DES simulation on the free surface of the cylinder is created with slightly more delay than the LES-WALE simulation.

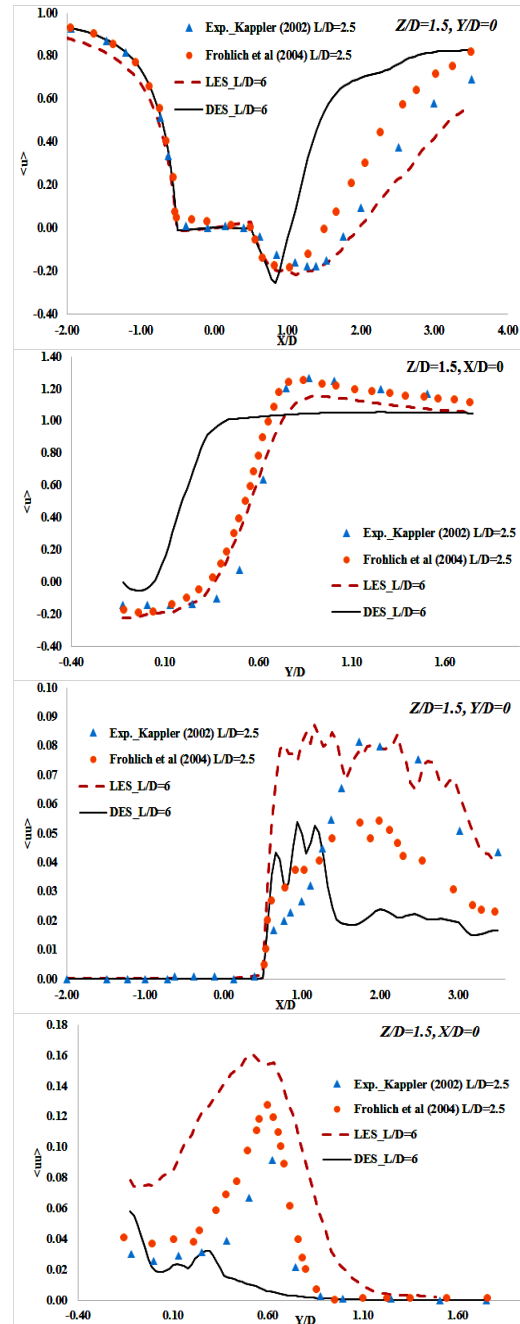


**Fig. 9. Comparison of the streamwise mean velocities (two top) and corresponding fluctuations (two bottom).**

Figure 12 shows instantaneous picture of vortex shedding close to the ground plate and comparison of both the LES-WALE and Zonal-DES results with experimental (Kappler, 2002) which were performed for the finite cylinder with  $L/D=2.5$  and  $Re=4.3 \times 10^4$ . The results of present work are instantaneous vorticity measured in the wall-adjacent cell. These results also qualitatively show better agreement for the LES-WALE rather than the

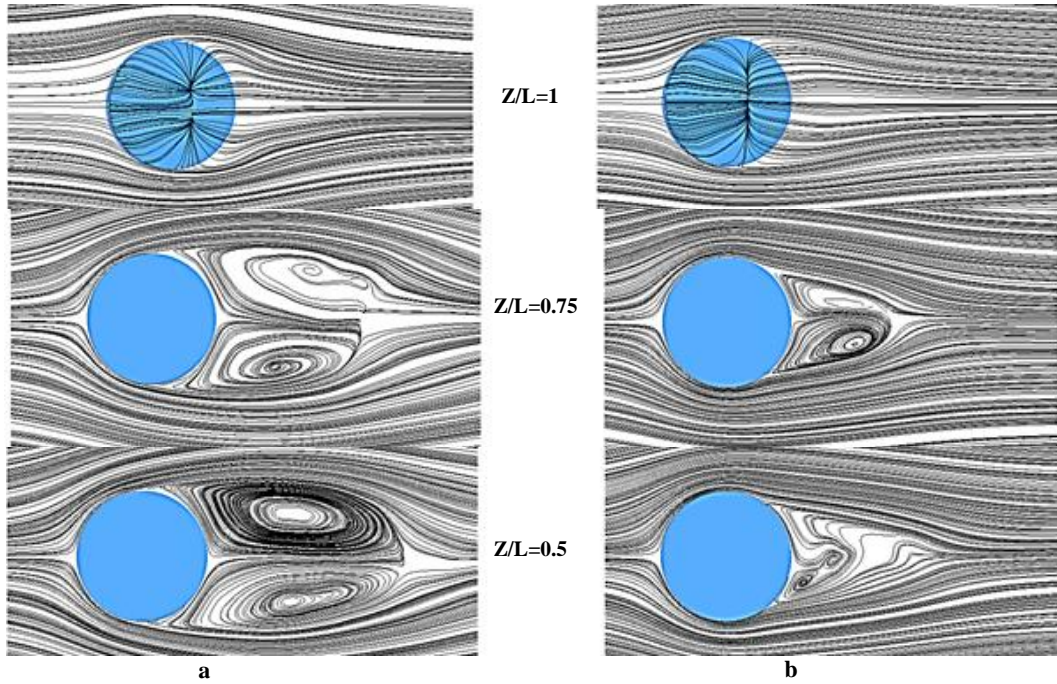


Fig. 11. Time-averaged streamlines projected on several XY- planes, (a) LES-WALE, (b) Zonal- DES.

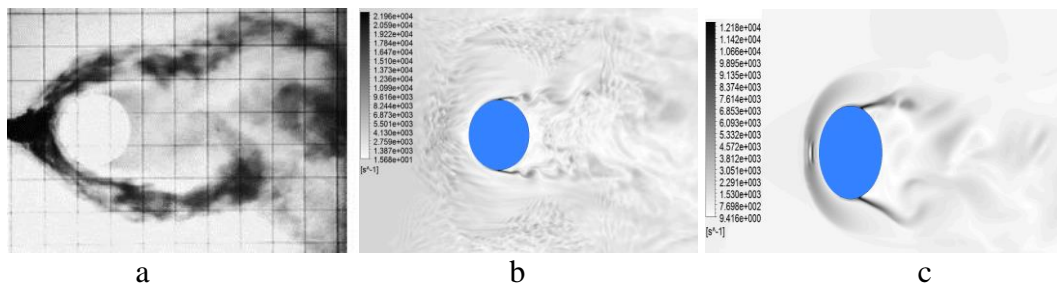


Fig. 12. Comparison of the instantaneous vortex shedding close to the ground plate. a) visualization by means of a tracer in the experiment “Kappler (2002)”, b) LES-WALE, c) Zonal-DES.

Zonal-DES turbulence model with the references.

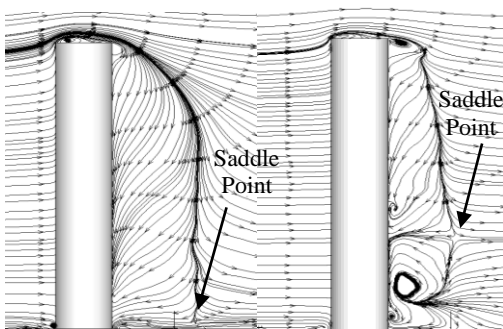
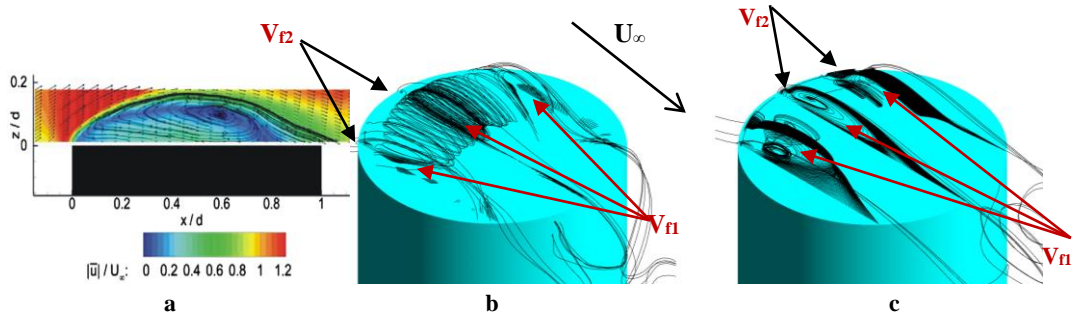


Fig. 10. Near wake visualized with streamlines in plane  $y=0$ , (a) LES-WALE (b) Zonal-DES.

Flow around the free end of the finite circular cylinder has been studied by several authors. Hain *et al.* (2008) experimentally indicated the mean flow field in the vertical symmetry plane ( $y/D=0$ ) for lower height circular (with  $L/D=1$ ) and  $Re=1.1 \times 10^5$ . To more investigate the streamlines are projected on several Y-planes and qualitatively compared in figure 13 for both the simulations

using the fine grid and experimental results (Hain *et al.*, 2008). The flow on the top surface contains large recirculation region,  $V_{f1}$ , which is oriented at the leading edge of the cylinder and the secondary recirculation region,  $V_{f2}$ , which is a result of separation of the recirculation flow from  $V_{f1}$  on its way back to the leading edge. Note that the recirculating region,  $V_{f2}$ , does not stretch all the way to the leading edge of the cylinder, but it reattaches and the  $V_{f1}$  region takes over (K Krajnovic, 2011). This flow structure on the free end of the finite circular cylinder has been experimentally shown by (Salvador *et al.*, 2010). Figure 13 shows that both the turbulence models capture the vortex core lines,  $V_{f1}$  and  $V_{f2}$ . The mean reattachment line position on the centerline of present study is compared with results of Krajnovic (2011) in table 4 for the same aspect ratio ( $L/D=6$ ). It is found that prediction of this saddle point by the LES-WALE model is closer to the numerical results in K Krajnovic (2011) than the Zonal-DES model. Figures 14 show qualitative comparisons of the Reynolds shear stress results on top of the cylinder for both the LES-WALE and Zonal-DES turbulence models with the



**Fig. 13.** Time-averaged streamlines projected on several Y-planes, (a) tomographic PIV “Hain et al. (2008)” (b) LES-WALE, (c) Zonal-DES.

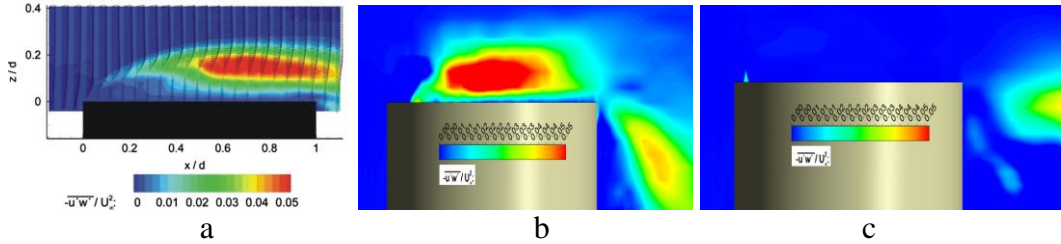


**Fig. 14.** Reynolds shear stress in the vertical symmetry plane ( $y/D=0$ ), (a) tomographic PIV “Hain et al. (2008)” (b) LES-WALE (c) Zonal-DES.

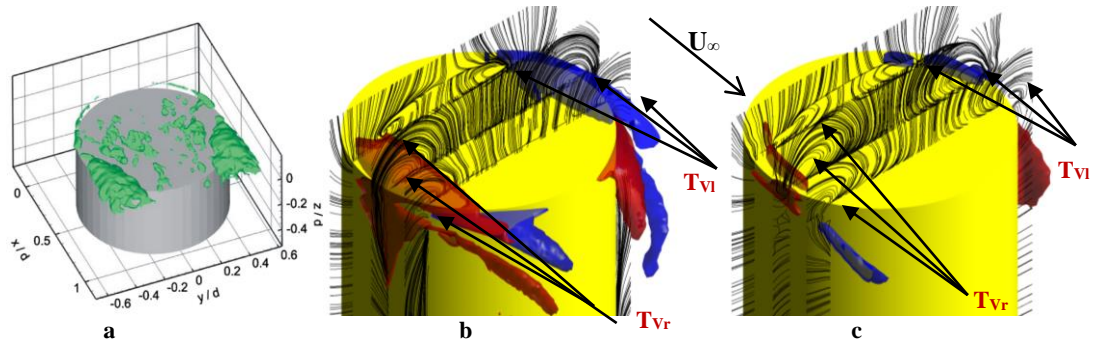


**Fig. 15.** Time-averaged streamlines projected on several X-planes, and time-averaged vorticity  $x = \pm 1750 [s^{-1}]$  iso-surface, (a) tomographic PIV “Hain et al. (2008)” (b) LES-WALE, (c) Zonal-DES.

experimental results (Hain *et al.*, 2008). Again, the accuracy of the LES-WALE model is observed in capturing these quantities rather than the Zonal-DES turbulence models.

**Table 4** Location of the reattachment saddle point on the center line of the free-end surface ( $L/D=6$ )

“K Krajnovic (2011)”	$X/D = 0.325$
LES-WALE	$X/D = 0.35$
Zonal-DES	$X/D = 0.25$

One of the most important flow structures on the top surface of the finite cylinder is formation of two strong tip vortices, right tip vortex,  $T_{Vr}$ , and left tip vortex,  $T_{Vl}$ . This structure on the top surface is shown in figures 15 by streamlines projected on several X-planes and time-averaged vortices  $x$  in iso-surfaces on the free end. Results are compared for both the LES-WALE and Zonal-DES models using the fine grid. Both simulations are able to capture this structure, but it seems that the tip

vortices simulated by the LES-WALE model is created sooner and stronger than the Zonal-DES model on the top surface. Producing more eddy viscosity by the Zonal-DES model respect to the LES-WALE model is the main reason of this phenomenon which diminishes the vortex strength. The tip vortices formation for the present solution are also compared with those of experimental results (Hain *et al.*, 2008) for lower height circular (with  $L/D=1$ ) and  $Re=1.1 \times 10^5$  in figure 15. More accurate tip vortices structure captured by the LES-WALE model is observed.

To investigate the far wake flow, the time-averaged streamlines projected on several YZ-planes near the flat plate at various  $x$  sections are plotted in figure 16 for both the simulations using the fine grid. The time-averaged flow turning along the cylinder interacts with the downwash flow beyond the closure of the separation bubble. It results flow in the symmetry plane impinging on the ground plane. After the impingement, the flow is pushed out of the symmetry plane to form the two counter-

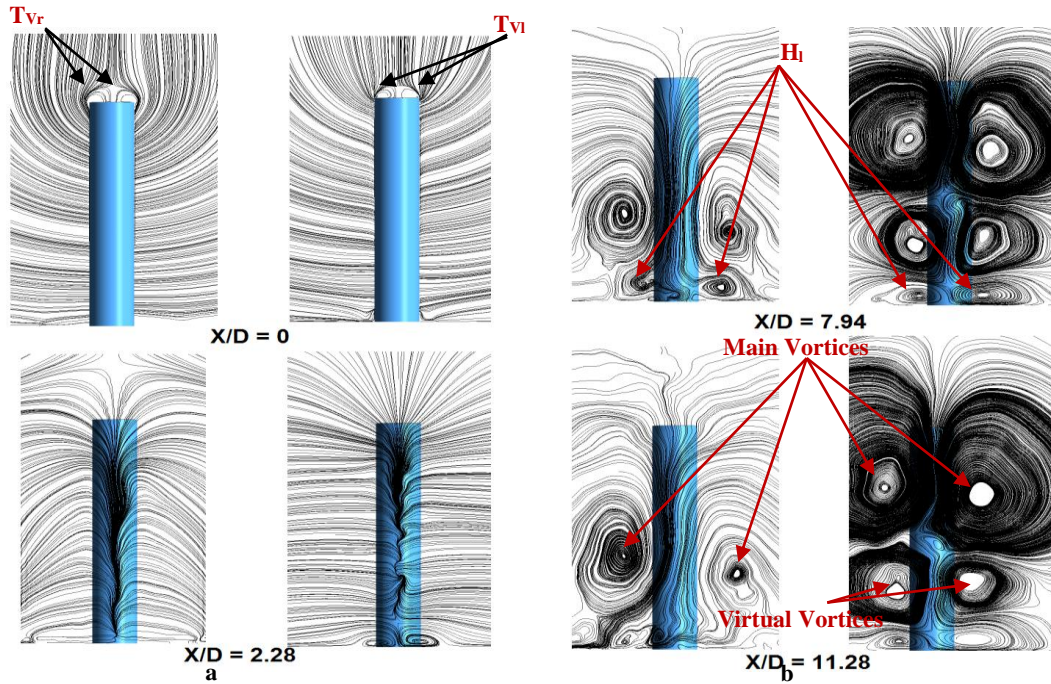


Fig. 16. Time-averaged streamlines projected on several YZ-planes, (a) LES-WALE, (b) Zonal-DES.

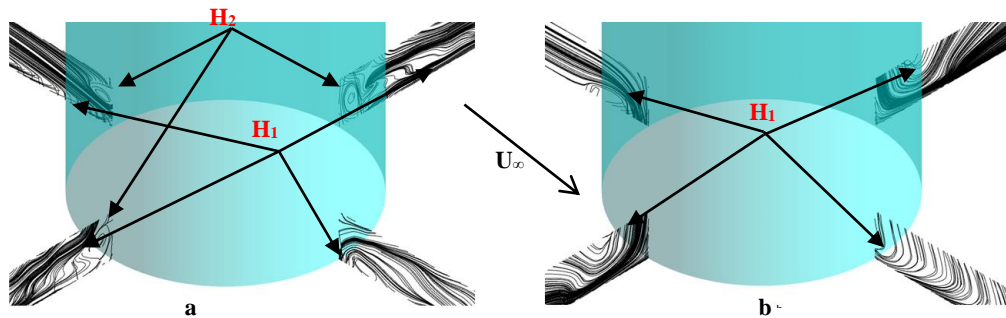


Fig. 17. Time-averaged streamlines projected on several planes near the ground, (a) LES-WALE, (b) Zonal-DES.

rotating vortices, “(Krajnovic 2011; Sumner, 2013)”. At  $X/D=0$ ,  $Tv_l$  and  $Tv_r$  captured by both the turbulence models are seen again. These tip vortices are origin of formation of the main vortices behind the cylinder where are forming by both the simulations at  $X/D=2.28$ . At  $X/D=7.94$ , it is observed that these asymmetric vortices are completely formed and remained in  $X/D=11.28$ . Also, two main horseshoe vortices,  $H_1$ , are observed at the bottom of the cylinder. It is found that virtual eddy viscosity produced by the Zonal-DES turbulence model creates two virtual vortices which are shown in figure 16. The impingement of the flow at the bottom of the cylinder causes a main horseshoe vortex,  $H_1$ , and a secondary horseshoe vortex,  $H_2$ , (figure 17). The two vortices are in opposite directions of rotation. This is in agreement with the topology of the horseshoe vortex system that was suggested by Baker (1980) and found earlier by Pattenden *et al.* (2005; 2007) The main horseshoe vortex,  $H_1$ , is captured with both the turbulence models but the secondary horseshoe

vortices,  $H_2$ , are just shown by the LES-WALE model.

The instantaneous horseshoe vortices are unsteady and move in all three spatial directions. A rather complete horseshoe vortex can be observed at the same time instances, for both the simulations in figure 18. Also, figure 18 compares the interaction of the vortices shedding at back of the cylinder and vortices down washing from the free end surface. This interaction between flow coming from the free end and the separated flow along the cylinder delays the separation point. Moreover, figure 18 shows that the LES-WALE model remains the shed vortices longer than the Zonal-DES model and forms larger reattachment region. This behavior is also seen in figure 19 which shows the comparison of the time-averaged vortices iso-surfaces for both the LES-WALE and Zonal-DES turbulence models. Reason of sooner vortices damping in the Zonal-DES simulations is producing of the additional eddy viscosity rather than the LES-WALE model.

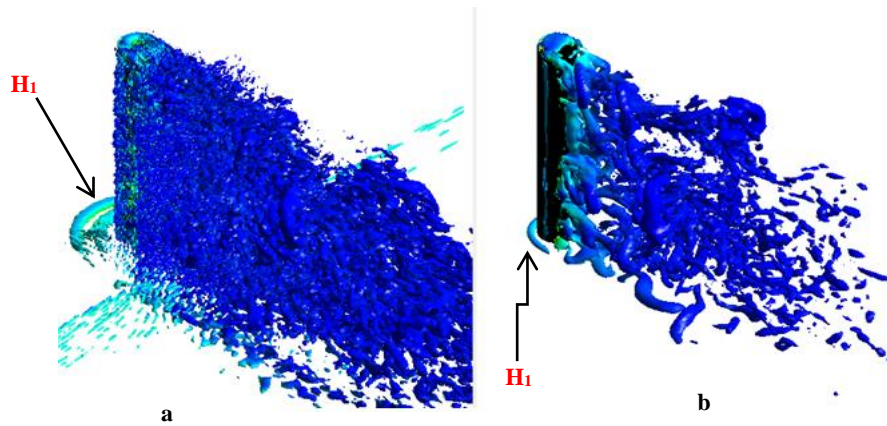


Fig. 18. Instantaneous iso-surface of velocity gradient  $Q = 250 [s^{-1}]$ , (a) LES-WALE, (b) Zonal-DES.

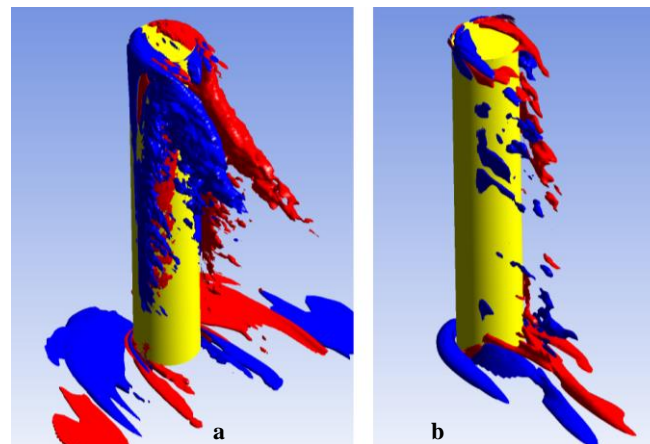


Fig. 19. Time-averaged vorticity  $x = \pm 500 [s^{-1}]$  iso-surface, (a) LES-WALE, (b) Zonal-DES.

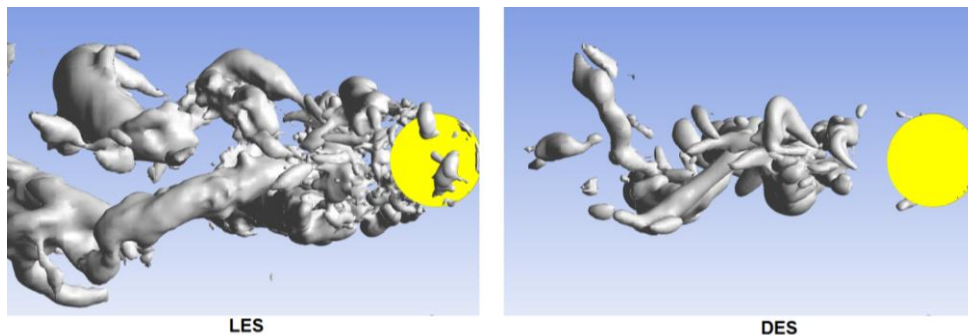


Fig. 20. Von-Karman vortices: Time-averaged pressure-Pressure = 2500 [Pa] iso-surface.

Unsteady flow over a cylinder causes von-Karman vortices. Formation of these shed vortices can be observed by plotting the time-averaged pressure iso-surface around the cylinder (Figure 20). It is shown that this structure is captured by both the simulations but the LES-WALE model shows longer vortices respect to the Zonal-DES model due to less calculated eddy viscosity.

Arc-shaped vortex, as schematically shown in figure 1, is one of the well-known structures generated by moving fluid over a finite cylinder. This phenomenon has been addressed for short finite cylinder by many researcher (Krajnovic 2011;

Agui *et al.* 1992; Pattenden *et al.* 2007; Sumner, 2013), previously. As reported by “K Krajnovic (2011)” the arc-vortex has a symmetric topology for  $L/D = 4$ . However, by increasing the aspect ratio, the shape of the vortex becomes more asymmetric. Figure 21 shows the arc-vortex is well captured by the LES-WALE simulations. If we take a look from top to the flow behind the cylinder in figure 11, it can be observed that the asymmetric wake region is well captured by both the LES-WALE and Zonal-DES models. According to the figures 13 and 15, it can be concluded that the root of formation of the arc are shedding of the fluid from the top of the cylinder into the low pressure wake region behind

the cylinder. Although this low pressure region is shown in both the simulations (e.g. see Figures 10, 11); however the Zonal-DES model cannot result the arc vortex phenomena.

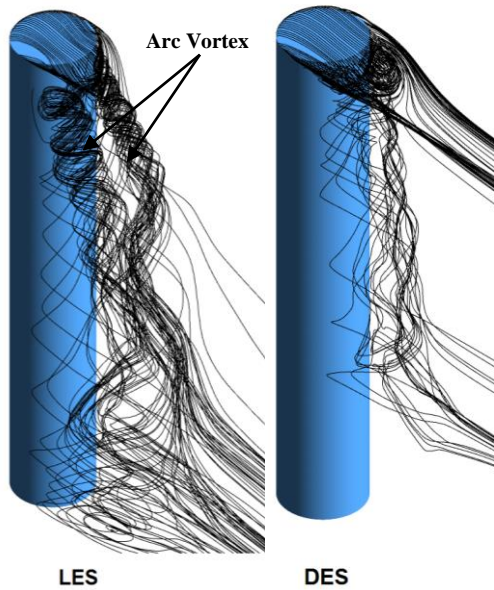


**Fig. 21.** Time-averaged streamlines projected Arc-shaped vortex.

### 6.3 Lateral and Drag Forces

Figure 22 represents the temporal behavior of the side force coefficient for both the LES-WALE and Zonal-DES turbulence models over 100 convective units  $D/U_\infty$  for the fine grids. The results predicted by the LES-WALE clearly shows an alternate vortex shedding of the separated flow whereas by using the Zonal-DES turbulence model, this shedding is distributed by lower frequency and amplitude. It is clearly found that the premature eddy viscosity in the DES model reduces the amplitude and frequency of the side force coefficient. The FFT (Fast Fourier Transformation) of the temporal signals of the side force in figure 22(b) reveals that there are two associated Strouhal numbers,  $St_1$  and  $St_2$ , in the flow over long finite cylinder. As mentioned before, these two Strouhal numbers are observed because of forming of two tip vortices in the flow over the finite cylinder (the main and secondary tip vortices). The main tip vortex with greater energy,  $St_1$ , causes the main separation over the cylinder and its pair with lower energy,  $St_2$ , makes secondary separation (see also Figs. 4 and 7). This matter has not been reported for the long finite circular cylinder up to now. It is shown that both the LES-WALE and Zonal-DES simulations can capture these points. The experimental studies performed by Park *et al.* (2002) revealed that the main vortex shedding frequency is at 47 Hz corresponding to a dimensionless frequency of  $St_1=0.141$ . This frequency was measured experimentally at  $X/D=3$ ,  $Y/D=2$ , and  $Z/L=0.5$  where are in the vicinity of the time-averaged shear-layer. Also Jensch *et al.* (2006) mentioned two Strouhal number for a short cylinder. To investigate the accuracy of the

simulations, the first and second calculated Strouhal numbers are listed in table 5. This comparison shows that the LES-WALE simulation has the least error for  $St_1$  using the fine grid, approximately 7%. The shedding frequencies are calculated 45.45 [Hz] and 37.04 [Hz] for the LES-WALE and Zonal-DES models using the fine grid, respectively. According to the frequency experimentally reported in Park *et al.* (2002) as 47 [Hz], it is found that the LES model has more accurate results.

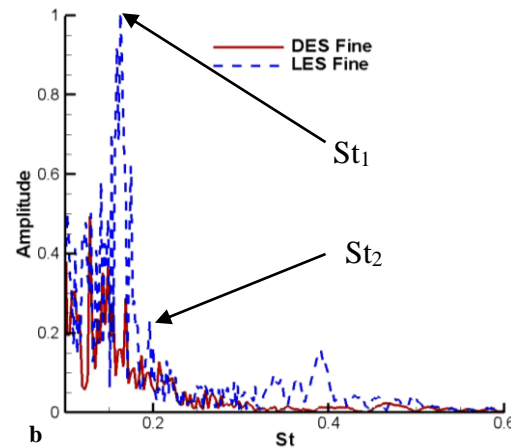
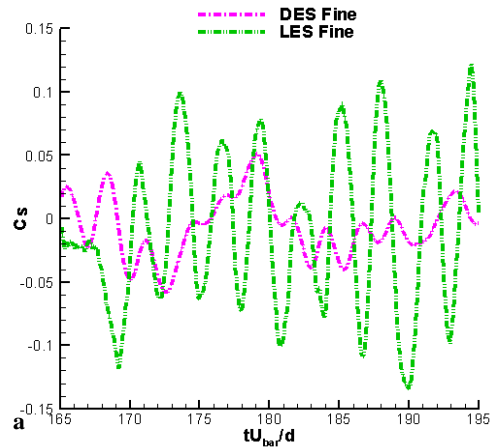


**Fig. 22.** (a) Global side force coefficients, (b) FFT of side force coefficients.

**Table 5 Comparison of the Strouhal numbers**

Authors	Method	L/D	$St_1$	$St_2$
“Jensch <i>et al.</i> (2006)”	Exp.	2	0.162	0.2
“Frohlich <i>et al.</i> (2003)”	LES	2.5	0.160	-
“Park <i>et al.</i> (2002)”	Exp.	6	0.141	-
Present Study	LES	6	0.151	0.196
Present Study	DES	6	0.127	0.149

For more investigation, figure 23 shows comparison of drag coefficient for both the LES-WALE and Zonal-DES models. The mean drag coefficient is predicted about 0.75 by the LES-WALE model and about 0.28 by the Zonal-DES model. The results show that the Zonal-DES model misses much of the pressure drag due to delayed boundary layer separation and smaller unsteady recirculation flow

(Frederich *et al.*, 2008). As mentioned by Baban *et al.* (1991), the unsteady drag is induced by the unsteady recirculation flow behind the cylinder and greater unsteady recirculation region causes greater drag force, the present results also confirm their conclusion. As shown in figures 9 and 10 the LES-WALE turbulence model predicts the recirculation region larger than the Zonal-DES turbulence model and then causes the greater drag force. Also the drag force predicted by both the simulations is greater than the side force. Moreover, good agreement between the calculated pressure coefficients reported by the LES-WALE turbulence model with measured data in figure 4 shows that the drag force determined by the LES-WALE turbulence model has more accuracy than the Zonal-DES model.

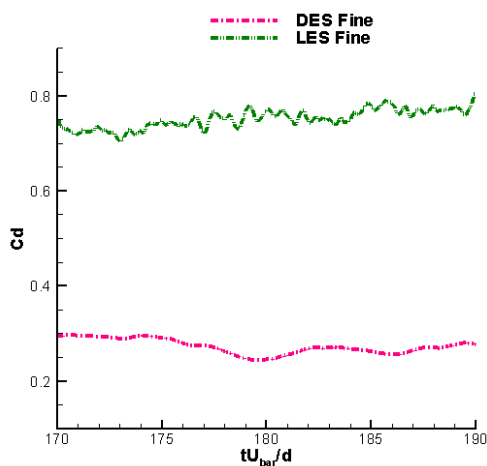


Fig. 23. Global drag force coefficients.

## 7. CONCLUSION

The three-dimensional unsteady flow field around a finite circular cylinder standing in a flat-plate boundary layer has been predicted using two different numerical turbulence approaches; the wall-adapted local eddy-viscosity LES (LES-WALE) and the Zonal Detached-Eddy Simulation (Zonal-DES). The investigations have been carried out using the coarse and fine computational grids around the finite circular cylinder with a diameter of  $D=3$  mm and a length-to-diameter ratio of  $L/D=6$  which based on the Reynolds number  $2 \times 10^4$ , approximately.

In the present study, surface pressure, flow structure, velocity distribution and lateral and drag forces on the finite cylinder have been studied by both the turbulence models. Comparison of the time-averaged surface pressure coefficient with the experimental data shows that the Zonal-DES turbulence model has more delay in capturing of the pressure recovery region respect to the LES-WALE turbulence model. The Zonal-DES model captures narrower wake and smaller reattachment region compared to the LES-WALE model. The time-averaged components of the velocity vector and the Reynolds stress tensors have been qualitatively compared between two simulations. It is found that

both the LES-WALE and Zonal-DES models have a similar behavior but the shed wake at back of the cylinder captured by the LES-WALE model is stronger than the Zonal-DES model because of producing additional eddy viscosity by the Zonal-DES model. It has been also shown that both the turbulence models are able to obtain two strong tip vortices structure, but the tip vortices simulated by the LES-WALE model is created sooner and stronger than those by the Zonal-DES simulation on the free end. The main horseshoe vortex is captured by both the turbulence models, however, the secondary horseshoe vortices are found just by the LES-WALE model in the same grid. Also, it is seen that the LES-WALE model keeps the shed vortices longer than the Zonal-DES model and forms the larger reattachment region due to less calculated eddy viscosity by the LES-WALE model. Moreover, the virtual eddy viscosity produced by the Zonal-DES turbulence model creates two virtual vortices behind the cylinder. Comparison between the vortex shedding frequencies shows that the LES-WALE gives more accurate results than the Zonal-DES model for the coarse and fine grids.

It is found that all discrepancies between results of two turbulence models arise from produced premature eddy viscosity by the DES model due to its grid sensitivity.

For the first time, the present study has shown the locations of forming  $St_1$  and  $St_2$  around the long finite cylinder using numerical methods. Moreover, in the same grid structure which the LES-WALE turbulent model gives accurate results, the Zonal-DES model does not present reliable results. Thus, to achieve proper results by the Zonal-DES turbulence model, it is required different grid structure quality respect to the LES-WALE.

## REFERENCES

- Afgan, I., C. Moulinec, R. Prosser and D. Laurence (2007). Large eddy simulation of turbulent flow for wall mounted cantilever cylinders of aspect ratio 6 and 10. *Int. J. Heat Fluid Flow* 28(4), 561–574.
- Afgan, I., C. Moulinec and D. Laurence (2006). Large eddy simulation of flow over a vertically mounted finite cylinder on a flat plate, in *Conference on Modelling Fluid Flow. The 13th International Conference on Fluid Flow Technologies, Budapest, Hungary.*
- Agui, J. H. and J. Andreopoulos (1992). Experimental investigation of a three-dimensional boundary layer flow in the vicinity of an upright wall mounted cylinder. *ASME Trans. J. Fluids Eng.* 114, 566–576.
- Baban, F. and R. M. C. So (1991). Recirculating flow behind and unsteady forces on finite-span circular cylinders in a cross-flow. *J. Fluids Struct.* 5(2), 185–206.
- Baker, C. J. (1980). The turbulent horseshoe vortex, *J. Wind Eng. Ind. Aerodyn.* 6(1), 9–23.

- Chen, C. J. and S.-Y. Jaw (1998). *Fundamentals of turbulence modeling*. Taylor & Francis.
- Fröhlich, J., W. Rodi (2003). LES of the flow around a cylinder of finite height. *In: Proc. of 3rd Int. Symp. on Turbulence and Shear Flow Phenomena*, Sendai, Japan.
- Fröhlich, J. and W. Rodi (2004). LES of the flow around a circular cylinder of finite height. *Int. J. heat fluid flow* 25(3), 537–548.
- Frederich, O., E. Wassen and F. Thiele (2008). Prediction of the Flow Around a Short Wall-Mounted Finite Cylinder using LES and DES1. *JNAIAM* 3(3–4), 231–247.
- Germano, M., U. Piomelli, P. Moin and W. H. Cabot (1991). A dynamic subgrid-scale eddy viscosity model. *Phys. Fluids A Fluid Dyn.* 3, 1760.
- Giordano, R., A. Ianiro, T. Astarita and G. M. Carlomagno (2012). Flow field and heat transfer on the base surface of a finite circular cylinder in cross-flow. *Applied Thermal Engineering* 49, 79-88.
- Heseltine, J. L. (2011). Flow around a circular cylinder with a free end.
- Hain, R., C. J. Kahler and D. Michaelis (2008). Tomographic and time resolved PIV measurement on finite cylinder mounted on a flat plate. *Exp. Fluids* 45, 715-724.
- Igbalajobi, A., J. F. McClean, D. Sumner and D. J. Bergstrom (2012). The effect of a wake-mounted splitter plate on the flow around a surface-mounted finite-height circular cylinder. *J. Fluids Struct.*
- IM, H.-S. and G.-C. Zha (2011). Delayed Detached Eddy Simulation of a Stall Flow Over NACA0012 Airfoil Using High Order Schemes. *AIAA Pap.* 1297.
- Lungo, G. V., L. M. Pii and G. Buresti (2012). Experimental investigation on the aerodynamic loads and wake flow features of a low aspect-ratio circular cylinder. *J. Fluids Struct.* 28, 279–291.
- Jensch, M., M. Brede, F. Richter and A. Leder (2006). Verwendung des Time-Resolved Stereo-PIV Messsystems zur Ermittlung zeitaufgelöster Geschwindigkeitsfelder im Nachlauf eines Kreiszyllinders. *In: Lasermethoden in der Strömungsmesstechnik*, PTB Braunschweig.
- Johnston, C. R. and D. J. Wilson (1996). A vortex pair model for plume down wash in to stack wakes. *Atmospheric Environment* 31, 13–20.
- Kappler, M. (2002). Experimentelle Untersuchung der Umströmung von Kreiszyllindern mit ausgeprägten dreidimensionalen Effekten. *Ph.D. thesis*, Institute for Hydromechanics, University of Karlsruhe.
- Krajnovic, S. (2011). Flow around a tall finite cylinder explored by large eddy simulation. *J. Fluid Mech.* 676, 294–317.
- Kawamura, T., M. Hiwada, T. Hibino, I. Mabuchi and M. Kumada (1984). Flow around a finite circular cylinder on a flat plate (cylinder height greater than turbulent boundary layer thickness). *Bull. JSME* 232, 2142–2151.
- Lilly, D. K. (1992). A proposed modification of the Germano subgrid-scale closure method. *Phys. Fluids A Fluid Dyn.* 4, 633.
- Liu, Y., R. M. C. So and Z. X. Cui (2005). A finite cantilevered cylinder in a cross-flow. *J. Fluids Struct.* 20(4), 589–609.
- Menter, F. R. (1994). Two-equation eddy-viscosity turbulence models for engineering applications. *AIAA J.* 32(8), 1598–1605.
- Menter, F. R., M. Kuntz and R. Langtry (2003). Ten years of industrial experience with the SST turbulence model. *Turbul. heat mass Transf.* 4, 625–632.
- Menter, F. R. and M. Kuntz (2004). Adaptation of eddy-viscosity turbulence models to unsteady separated flow behind vehicles. *Aerodyn. heavy Veh. Truck. buses, trains* 19, 339–352.
- Nicoud, F. and F. Ducros (1999). Subgrid-scale stress modelling based on the square of the velocity gradient tensor. *Flow, Turbul. Combust.* 62(3), 183–200.
- Pattenden, R. J., S. R. Turnock and X. Zhang (2005). Measurements of the flow over a low-aspect-ratio cylinder mounted on a ground plane. *Exp. Fluids* 39(1), 10–21.
- Pattenden, R. J, N. W. Bressloff, S. R. Turnock and X. Zhang (2007). Unsteady simulations of the flow around a short surface-mounted cylinder. *Int. J. Numer. methods fluids* 53(6), 895–914.
- Palau Salvador, G., T. Stoesser, J. Fröhlich, M. Kappler and W. Rodi (2010). Large eddy simulations and experiments of flow around finite-height cylinders. *Flow. Turbul. Combust.* 84(2), 239–275.
- Park, C. W. and S. J. Lee (2000). Free end effects on the near wake flow structure behind a finite circular cylinder. *Journal of Wind Engineering and Industrial Aerodynamics* 88, 231-426.
- Park, C. W. and S. J. Lee (2002). Flow structure around a finite circular cylinder embedded in various atmospheric boundary layers. *Fluid Dyn. Res.* 30(4), 197–215.
- Philippe, R. (2001). Young-Person’s Guide to Detached-Eddy Simulation Grids.
- Roh, S. and S. Park (2003). Vortical flow over the free end surface of a finite circular cylinder mounted on a flat plate. *Exp. Fluids* 34(1), 63–67.
- Rostamy, N., D. Sumner, D. J. Bergstrom and J. D. Bugg (2012). Local flow field of a surface-mounted finite circular cylinder. *J. Fluids*

- Struct.* 34, 105–122.
- Smagorinsky, J. (1963). GENERAL CIRCULATION EXPERIMENTS WITH THE PRIMITIVE EQUATIONS: I. THE BASIC EXPERIMENT. *Mon. Weather Rev.* 91(3), 99–164.
- Spalart, P. R., S. Deck, M. L. Shur, K. D. Squires, M. K. Strelets and A. Travin (2006). A new version of detached-eddy simulation, resistant to ambiguous grid densities. *Theor. Comput. Fluid Dyn.* 20(3), 181–195.
- Spalart, P. R., W. Jou, M. Strelets and S. Allmaras (1997). Comments of feasibility of LES for wings, and on a hybrid {RANS/LES} approach.
- Strelets, M. (2001). Detached eddy simulation of massively separated flows.
- Sumner, D. (2013). Flow above the free end of a surface-mounted finite-height circular cylinder: A review. *J. Fluids and Structures* 43, 41-63.
- Vengadesan, S. and P. Nithiarasu (2007). Hybrid LES—Review and assessment. *Sadhana* 32(5), 501–511.
- Viswanathan, A. K. (2006). Detached Eddy Simulation of Turbulent Flow and Heat Transfer in Turbine Blade Internal Cooling Ducts. *Virginia Polytechnic Institute and State University*.
- Williamson, C. H. K. (1996). Vortex dynamics in the cylinder wake. *Annu. Rev. Fluid Mech.* 28(1), 477–539.
- Williamson, C. H. K. (1985). Evolution of a single wake behind a pair of bluff bodies. *J. Fluid Mech.* 159, 1–18.
- Zdravkovich, M. M. (2003). *Flow around Circular Cylinders: Volume 2: Applications 2*. Oxford University Press.